Time-resolved particle image velocimetry used in the investigation of cavitation bubble dynamics

Alfred Vogel and Werner Lauterborn

The temporal evolution of the velocity field of an unsteady fluid flow can be tracked by combining particle image velocimetry and high speed photography. We used this technique to investigate the flow around cavitation bubbles during their collapse near a solid boundary. The light source was an argon laser with an external acoustooptic deflector which produces series of short pulses. Using a drum camera for high speed photography, we achieved a temporal resolution of 10 kHz and a spatial resolution of better than 2 points/mm^2. Velocities could be determined without directional ambiguity in a range from 2 to 30 m/s.

I. Introduction

There has been a trade-off between the possibility of recording whole velocity fields with laser speckle velocimetry or particle image velocimetry (PIV)[1–7] and the ability of techniques such as laser Doppler velocimetry[8,9] to track the temporal evolution of a fluid flow at a single point. To overcome this limitation, we conceived an experimental arrangement for time-resolved PIV, where PIV is combined with high speed photography. The technique was applied to investigate the unsteady flow around asymmetrically collapsing cavitation bubbles.

The interest in the dynamics of cavitation bubbles in liquids arises from their destructive action on solid surfaces. A bubble collapsing near a solid boundary develops a high speed liquid jet which moves toward the boundary. As the maximum jet velocity may easily exceed 100 m/s, the water hammer pressure produced by the jet impinging on the surface is regarded as a cause of cavitation erosion. This picture has emerged from high speed photographic experiments[10–14] and numerical calculations.[15] Until recently, only data about the bubble shape could be obtained both experimentally and numerically. A more detailed investigation of jet formation should include the velocity and pressure field around the bubble. Theory has already succeeded in supplying path lines and pressure contours in the neighborhood of collapsing bubbles,[16] but, as already encountered in the shape calculation, the development of the jet can only be followed until it hits the opposite bubble wall. Experiments are notoriously difficult in this area, as a plane in the liquid containing the center of the collapsing bubble has to be monitored at high spatial and temporal resolutions. The repetition rate of the measurement determining the temporal resolution is set by the lifetime of the bubble of only ~1 ms and should exceed 10,000 s^{-1}. The spatial resolution is set by the size of the collapsed bubble which usually is smaller than 0.1 mm and should reach several points of measurement per mm^2. As described below, these objectives could be reached by time-resolved PIV using an argon laser as the light source and a drum camera for high speed photography.

II. Time-Resolved Particle Image Velocimetry

A. Recording of PIV Photographs

The scheme for recording PIV photographs is quite simple (see Fig. 1). The fluid is seeded with microparticles serving as light scatterers, the density of which is adjusted to that of the fluid. A plane in the fluid is illuminated by a thin light sheet, and the particle distribution in this plane is imaged onto photographic film. Since the scattering particles follow the fluid flow, they are recorded as a chain of particle images when the film is multiply exposed. The projection of the fluid velocity vector into the observation plane can be calculated from the direction of each chain, the distance between the particle images and the time between successive exposures.

The temporal evolution of the flow field can be measured by taking a series of multiple exposure photographs. For this, the light source should be able to produce regular bursts of intense pulses of short dura-

The authors are with University of Goettingen, Third Physics Institute, Buergerstrasse 42, D-3400 Goettingen, Federal Republic of Germany.

Received 17 September 1987.
0003-6935/88/091869-00$02.00/0.

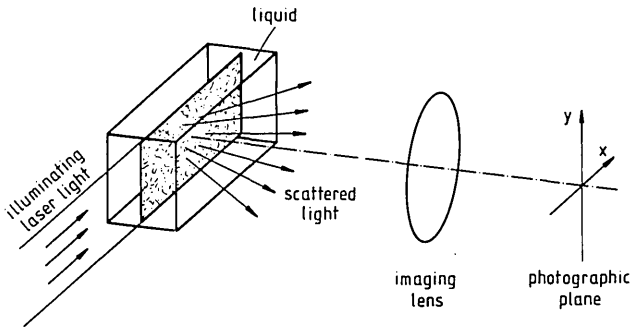

Fig. 1. Basic scheme for the recording of photographs for particle image velocimetry (PIV).

tion and a high rate of repetition. At present, there are no light sources available which meet all these requirements. We applied an argon-ion laser whose continuous light output is externally chopped by an acoustooptic deflector (see Fig. 2). It delivers pulses with a high repetition rate of up to 1 MHz although, unfortunately, with very low pulse energy.

PIV usually suffers from directional ambiguity: the magnitude of the velocity vector can be determined correctly, but its direction is ambiguous to within a sign error.[7,17] Combining PIV and high speed photography, this problem can easily be overcome by using a drum camera to record the picture series.[7] In this camera type, the images are separated by the film movement. This leads to a distance d_0 between the individual images in each particle image chain, when there is no fluid motion. With fluid motion, the distance between the particle images is changed and the orientation of the image chains is altered as well. To avoid directional ambiguity, the relation

$$v_f > M v_{max} \tag{1}$$

should be held, where v_f is the film velocity, v_{max} is the maximum fluid velocity, and M is the magnification of the lens. In this case, all particle images are shifted in the same direction with respect to the image recorded first. The distance between adjacent images is larger or smaller than d_0 depending on the direction of the flow.

The velocity dynamic range of PIV is usually determined by ensuring that for a measurement the spacing between the particle images is well resolved and that the direction and velocity of the particle movement is approximately constant between successive exposures. Lourenco has shown[18] that the dynamic range is thereby limited to about $(v_{max} - v_{min})/v_{min} = 7$. In PIV with moving film, however, the upper limit of the measurement range is, according to Eq. (1), defined by the film velocity v_f. The lower limit depends on the accuracy in determining the separation between particle images. Therefore, the dynamic range may be considerably larger than in conventional PIV.

B. Evaluation of PIV Photographs

At present, mainly two basic concepts are employed for the evaluation of PIV photographs:

(1) Evaluation via the diffraction pattern. A small part of the photograph is illuminated with a coherent plane wave, typically an unexpanded He–Ne laser beam. Then in the back focal plane of a converging lens Young's fringes modulating a speckle pattern are observed with a spacing and an orientation directly

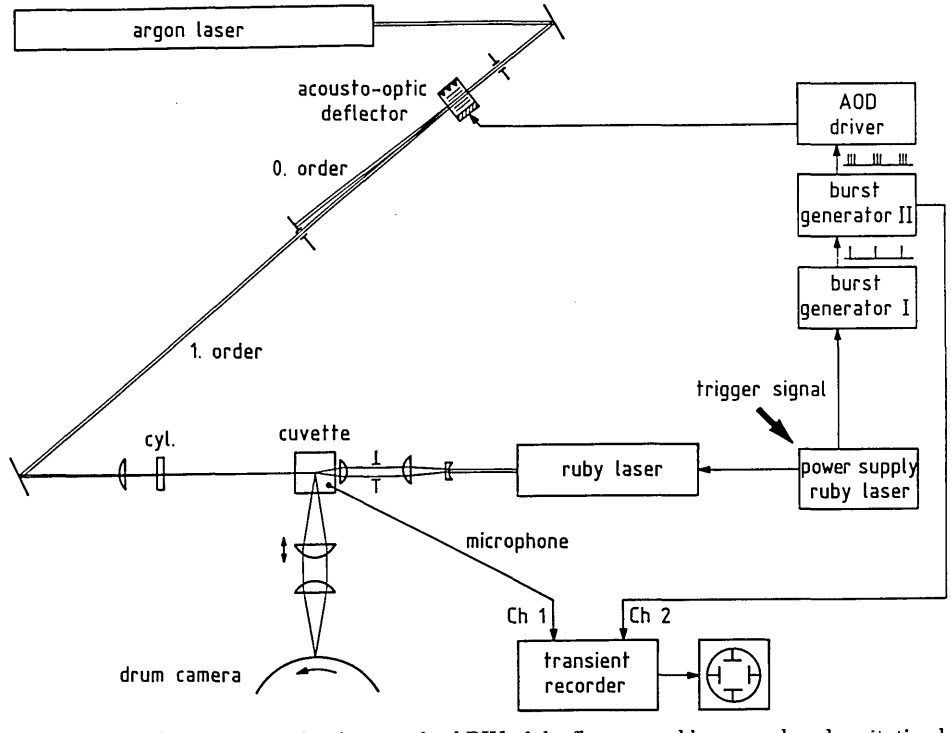

Fig. 2. Experimental arrangement for time-resolved PIV of the flow around laser-produced cavitation bubbles.

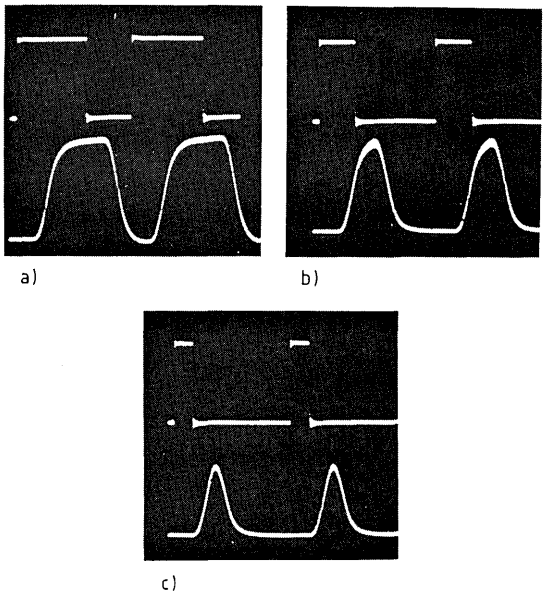

Fig. 3. Shape of the light pulses from the acoustooptic deflector (bottom) and the corresponding driving signal (top) with a duration of (a) 2 μs, (b) 1 μs, and (c) 0.5 μs. The pulse energy is 6 μJ in (a) 3 μJ in (b), and 1.5 μJ in (c).

related to the fluid motion. The information on the velocity vector is usually extracted from the fringe pattern by digital image processing (see Refs. 1–5 and the review in Ref. 19).

(2) Direct evaluation by individual inspection or digital image processing.[20–22] This approach is useful as long as the density of scatterers is low and the particle image chains can be clearly identified. Besides, these methods are also useful if multiple exposure is substituted by long time exposure. In this case, the particle images are blurred out into stripes, the length and orientation of which gives the local velocity vector.[23–25]

The evaluation of the diffraction pattern is difficult, when only a very small area of the multiple exposure photograph is illuminated to achieve high spatial resolution. Then there are only a few particle chains in the interrogation area and cross interference of noncorresponding particle images produces fringe patterns which do not reflect the particle shift between exposures, but rather the particle distribution in the medium. According to Lourenco,[18] flawless evaluation of a test point will only be possible if more than three particle chains are situated in the interrogation spot. On the other hand, the information content of every single chain should be used to optimize the spatial resolution of the velocity field in the vicinity of the cavitation bubble. Therefore, direct evaluation of the multiple exposure photographs was considered better suited than evaluating the diffraction pattern.

Direct evaluation by digital processing requires automatic identification of particle images belonging together and rejection of test points where the particle images cannot be arranged in chains. However, a test point is often rejected in digital image processing when individual inspection still permits definite identification of the particle image chains by utilizing *a priori* knowledge about the fluid flow (see, e.g., Ref. 20). Investigating cavitation bubble dynamics, the main problem to face was not an extraordinarily large number of test points, but the achievement of optimal spatial resolution. Thus, no automatic evaluation system was built up. Instead, the photographs were drastically magnified and the enlarged prints were evaluated by individual inspection.

Multiple exposure of the photographs offers advantages over double exposure, since the identification of a chain of particle images is easier than that of a pair of images. Moreover, a test point can be used for evaluation, even if a single particle image cannot be detected. Long time exposures have much looser requirements with respect to the light source, but they have an important disadvantage. No distinction is possible between cases in which the length of a blurred image accounts for the whole exposure time and in which the particle has moved out of the light sheet during exposure.

III. Experimental Apparatus

A. Experimental Arrangement

The experimental arrangement is outlined in Fig. 2. The cavitation bubbles are produced by focusing pulses from a passively Q-switched ruby laser into a cuvette with distilled water. The intense laser pulses with 50-ns duration and 100–400-mJ pulse energy cause an optical breakdown at the focal point of the laser. This leads to the formation of spherical cavitation bubbles at a well-defined instant and location.[11,26]

The light source for PIV is a 3.6-W argon-ion laser. The laser beam is chopped by an acoustooptic deflector controlled by a combination of two burst generators. Thus, pulse trains of variable length, pulse separation, and repetition rate can be generated. Each PIV frame was exposed with a sequence of five pulses with 1-μs duration and 3-μs distance between successive pulses (see Fig. 3). The pulse energy was 3 μJ. The argon laser beam is expanded vertically by a cylindrical lens with 40-mm focal length and focused horizontally by a convex lens with a focal length of 400 mm. A light sheet of 15-mm height and 140-μm thickness is thereby produced in the plane, in which the center of the cavitation bubble is located. This plane is imaged into the film plane of the drum camera by a lens system with 75-mm focal length and an f/No. of 1.25. The diameter of the point spread function of the imaging system measured at its first zero is $\sim$20 μm. This value deviates from the value for a diffraction-limited lens system (1.6 μm) mainly because of the spherical aberrations introduced by the cuvette filled with water. Due to the large aperture of the optics, the depth of focus is only $\pm$200 μm, so that even small vibrations of the drum camera cause defocusing. Nevertheless, by damping the camera vibrations a film velocity of up to 70 m/s could be achieved without entailing significant image blur.

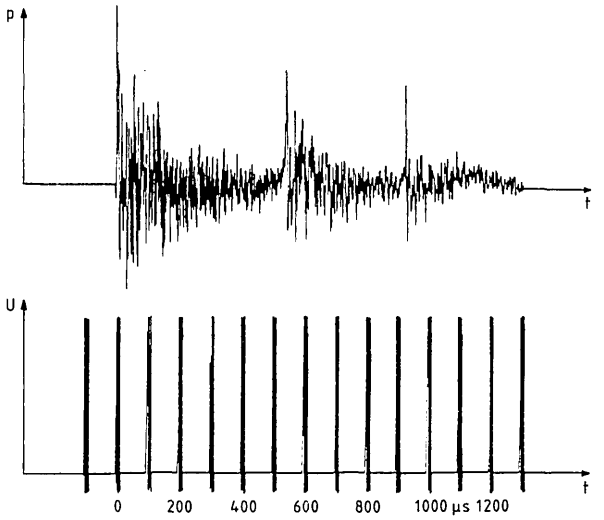

Fig. 4. Simultaneous recording of the acoustic signal of the laser-produced cavitation bubble (top) and the driving signal for the acoustooptic modulator (bottom). The first peak of the acoustic signal represents the shock wave emitted during optical breakdown, and the following peaks indicate the first and second bubble collapse.

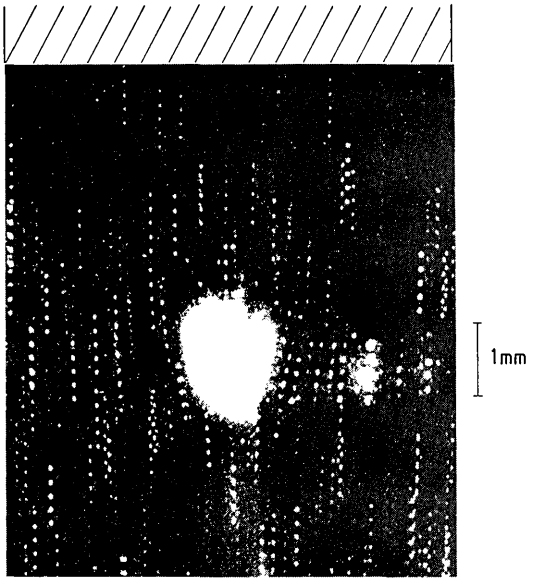

Fig. 5. PIV photograph of a cavitation bubble close to a solid boundary (hatched area) 7 μs before collapse, taken from a series with a 5-kHz framing rate, magnification of $M = 1$, and film velocity of 50 m/s. The maximum bubble radius is 1.8 mm and $\gamma = 2.4$.

The pictures were taken with Kodak Tri-X-Pan film and developed for 15 min in Kodak HC 110 (dilution B). Since the spectral sensitivity of this film is better at 514 nm than at 488 nm, we used the green line of the argon-ion laser, although the light scattering decreases with increasing wavelength.

Simultaneous to high speed photography, both the acoustic signal of the cavitation bubble and the driving signal for the illuminating light pulses are recorded with a transient recorder (see Fig. 4). By comparing both signals, the picture sequence of time-resolved PIV can exactly be related to the life cycle of the cavitation bubble.

B. Scattering Particles

The fluid was seeded with Vestamid particles[27] with an average diameter of $d_p = 25$ μm. These particles have almost the same refractive index as latex spheres ($n = 1.53$), but because of their polycrystalline structure, the scattering efficiency in the direction perpendicular to the light sheet is five times better. The density of Vestamid ($\rho = 1.01$–1.02 g/cm^3) almost equals the density of water. Therefore, the particles will follow the cavitation bubble-induced flow even in the final stage of the collapse, when the bubble wall is accelerated with $\sim 5 \times 10^6$ m/s^2.

To make the most effective use of the scattered light, the particle images should have approximately the same size as the area covered by the point spread function of the image optics. Assuming a magnification of $M = 1$, this can be seen by the following line of reasoning. In the domain of Mie theory, the gross scattering power is proportional to the cross section of the particles, but the angular distribution of the scattered light changes with particle size. The polycrystalline structure of the Vestamid particles implies that the size of the scattering elements remains constant when the particle diameter d_p is varied. The angular distribution will in this case be more or less independent of d_p. Therefore, the above-mentioned relationship between d_p and the amount of scattered light holds also for the scattering in the diffraction perpendicular to the illuminating laser beam. Thus, the light intensity in the particle image increases proportional to d_p^2 as long as d_p is smaller than the diameter d_{psf} of the point spread function. If d_p is larger than d_{psf}, an increase of d_p includes an enlargement of the area covered by the particle image and the mean image intensity approaches a constant.[28] Considering that d_{psf} is ~ 20 μm, the average particle diameter of 25 μm ensures optimum utilization of the scattered light. Larger particle sizes should be avoided, because small particles follow the flow better than large ones.

C. Limitations of the Technique

Preliminary trials indicated a minimum time of 0.5 μs necessary for each individual exposure of the multiple exposure photographs. Due to the film movement in the drum camera and to the fluid flow, the effective exposure time is shorter than the duration of the light pulses. The maximum possible exposure will be achieved when the particle image moves just one particle diameter during a pulse. With a particle diameter of 25 μm, a pulse duration of 1 μs ensures an effective exposure time of 0.5 μs up to a film velocity of 50 m/s. This sets the upper limit for the measurement range of the fluid velocity. There should be a minimum space of one particle image diameter between the particle images to make the evaluation possible. To ensure this in flow situations where film and particle images

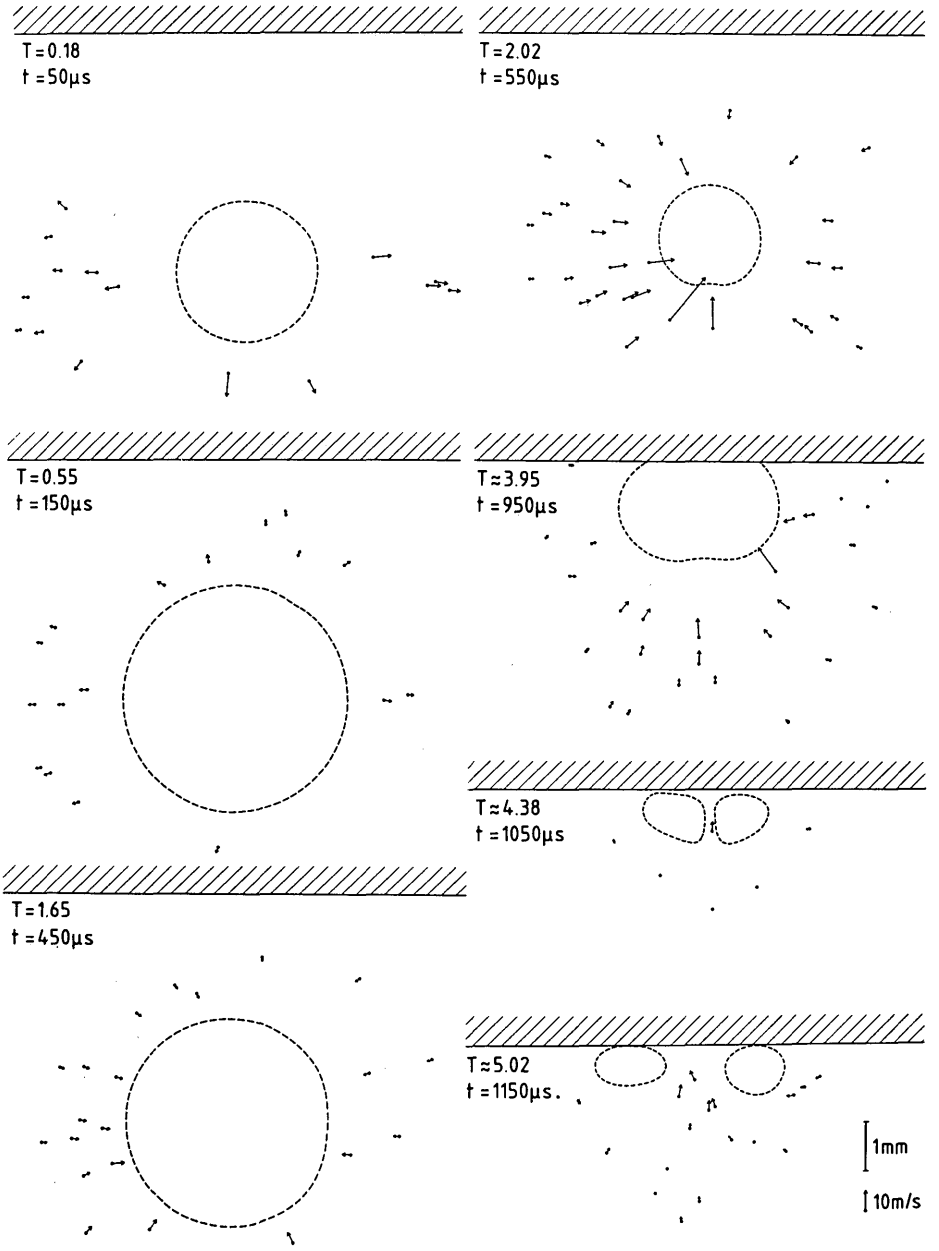

Fig. 6. Evolution of the velocity field around a laser-generated cavitation bubble close to a solid boundary. Subsequent diagrams are arranged in columns. The first collapse occurs between the fourth and the fifth picture, the second between the fifth and the sixth diagram. $\gamma = 1.9, R_{max} = 2.5$ mm. Time t is normalized by Rayleigh's collapse time T_c of a spherical bubble: $T = t/T_c$.

are moving in the same direction, the film velocity has to exceed the maximum velocity of the particle images. The largest detectable fluid velocity is connected to the film velocity by

$$v_{max} = \frac{3}{5M} v_f. \tag{2}$$

In deducing this relation, the assumption was made that the particles should not move more than $3d_p$ between two light pulses. Then, with $v \leq v_{max}$, the space between the particle images on the film is two to eight particle image diameters, depending on the flow direction. According to Eq. (2), fluid velocities up to 30 m/s can be detected at 50-m/s film velocity and a magnification of $M = 1$.

The highest possible framing rate ν_p is given by

$$\nu_p = \frac{v_f}{\text{height of picture}} = \frac{1}{M} \cdot \frac{v_f}{\text{height of object}}. \tag{3}$$

At an object volume of 10-mm vertical extension and a magnification of $M = 1$, a film velocity of 50 m/s yields a maximum framing rate of 5 kHz. It can be raised to 10 kHz, if the vertical dimension of the object volume is reduced to 7 mm and if the magnification is decreased to 5/7. In this case, the measurement range is shifted to higher velocities with an upper limit of 42 m/s. Further increase of the framing rate by reduction of the magnification does not seem useful, because it would drastically lower the accuracy of evaluation due to the course grain of the Tri-X-Pan film and the large diameter of the point spread function of the lens system. At 10-kHz framing rate, picture series consisting

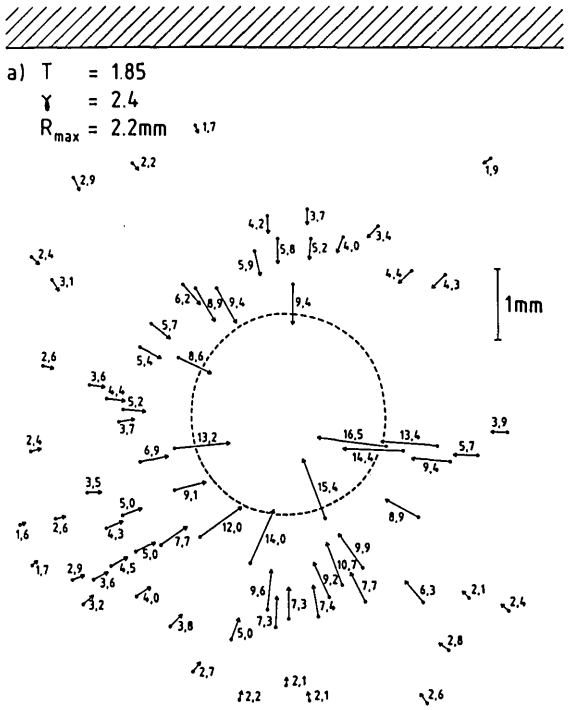

Fig. 7. Velocity field in the vicinity of a collapsing cavitation bubble at times (a) $T = 1.85$ and (b) $T = 2.08$. The velocity values are given in m/s. The diagrams are taken from two different series. (b) Evaluation of the photograph shown in Fig. 5.

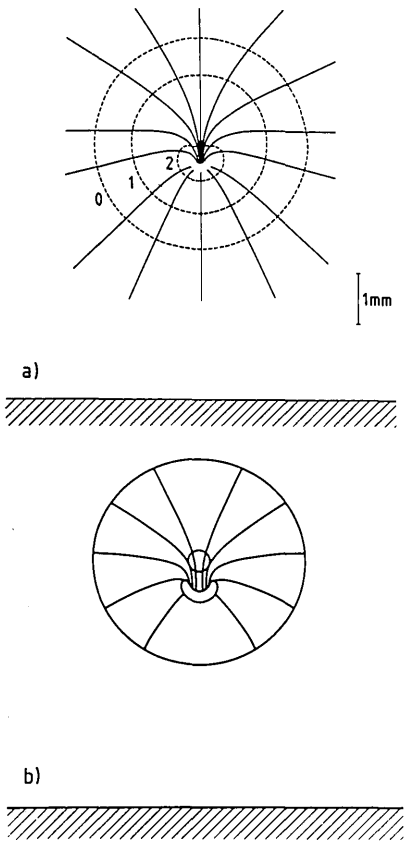

Fig. 8. (a) Experimentally obtained path line portrait of the flow around a collapsing cavitation bubble at $\gamma = 2.4$. Bubble shape 0 represents the bubble at maximum expansion, shape 1 belongs to $T = 1.85$, and shape 2 to $T = 2.08$. (b) Path line portrait for $\gamma = 2.4$ calculated numerically for several points on the wall of the collapsing bubble. Plot supplied by J. R. Blake. The dot in (a) and the small circle in (b) indicate the location of bubble formation.

of 300 frames can be taken with the drum camera, corresponding to a measurement time of 30 ms.

When the concentration of the scattering particles is increased, it becomes more and more difficult to produce pointlike optical breakdowns and spherical cavitation bubbles. On the other hand, the concentration of the scatterers should be as high as possible to ensure good spatial resolution in the analysis of the fluid velocity field. Spherical bubbles could be generated by the focused ruby laser pulses up to a concentration of 3×10^{10} scatterers/m^3, yielding a resolution of 2–3 measurement points/mm^2.

IV. Results

The most decisive parameter for jet formation during cavitation bubble collapse is the dimensionless distance between bubble and solid boundary:

$$\gamma = \frac{l}{R_{\max}} \cdot \tag{4}$$

Here l denotes the distance between the bubble center and the boundary, and $R_{\max}$ is the maximum radius of the cavitation bubble. Figure 5 shows a multiple exposure photograph of the flow around a cavitation bubble at $\gamma = 2.4$, taken from a series with a 5-kHz framing rate. The result of the evaluation of a series with 10-kHz framing rate is given in Fig. 6. As expected, the largest flow velocities are found on the side of the bubble where the jet is developing toward the solid boundary. The difference between the flow velocities on both sides of the collapsing bubble induces a movement of the whole bubble toward the solid boundary as well as jet formation in the same direction. The latter

is further indicated by the fact that at the end of the collapse the velocity vectors do not point toward the center of the bubble, but toward a spot close to its surface on the side opposite the solid boundary. The flow is thereby focused and strongly accelerated. The last diagram in Fig. 6 shows that, during the second collapse, a vortex ring is formed as a consequence of the jet flow through the bubble.

As indicated by Fig. 6, a satisfactory temporal resolution of the velocity field evolution in the vicinity of the bubble cannot be achieved even with the highest possible framing rate of 10 kHz. Besides, at an image scale of 5/7 the spatial resolution could not be made to exceed 1.5 measurement points/mm^2. Therefore, a different approach was attempted to increase spatial resolution. The image quality was improved by using a magnification of $M = 1$ and a framing rate of 5 kHz. The bubble dynamics was followed by combining pictures of different series taken at different stages of the bubble collapse. Figure 7 contains two velocity field representations for $\gamma = 2.4$ achieved by this procedure. In this case, spatial resolution is 2–3 measurement points/mm^2. The dynamic range of the velocity measurement is ~15:1.

Interpolation of the velocity fields in Fig. 7 results in the path line portrait in Fig. 8(a). Here, the solid boundary is drawn at the bottom of the diagram to facilitate comparison with the numerical results in Fig. 8(b). The path lines up to bubble shape 1 were obtained from Fig. 7(a), and Fig. 7(b) allowed their continuation up to shape 2. The path lines within shape 2 are speculative continuations of the flow pattern in the bubble vicinity. Figure 8(a) gives a good visualization of the fluid flow concentration during bubble collapse which results in jet formation. For a comparison of the experimental results with theory see Fig. 8(b) which shows a path line portrait for several points of the bubble surface calculated numerically by Blake *et al.*[16] for $\gamma = 2.4$.[20,29] There is good qualitative agreement between experimental and theory.

V. Conclusions

The velocity field of the fluid flow in the vicinity of a collapsing cavitation bubble has been investigated with the help of time-resolved particle image velocimetry. The rapid succession of multiply exposed frames is recorded by using a drum camera. The motion of the film with the rotating drum eliminates the ambiguity in the direction of the velocity present in conventional PIV. Furthermore, the dynamic range of measurable velocities is expanded. Velocities could be determined within a range of from <2 m/s to 30 m/s and within a field of 10×10 mm^2. A temporal resolution of 10 kHz and a spatial resolution of higher than 2 points/mm^2 have been achieved.

Time-resolved PIV offers new possibilities for the investigation of unsteady flows as it combines the advantages of conventional PIV, yielding the velocity field in a plane at one instant, and of laser Doppler anemometry which allows tracking of the temporal evolution of fluid flows at a single point.

We thank J. R. Blake, University of Wollongong, Australia, for supplying the plot of Fig. 8(b) prior to publication.

References

1. R. Grousson and S. Mallick, "Study of Flow Pattern in a Fluid by Scattered Laser Light," Appl. Opt. **16,** 2334 (1977).
2. D. B. Barker and M. E. Fourney, "Measuring Fluid Velocities with Speckle Patterns," Opt. Lett. **1,** 135 (1977).
3. T. D. Dudderar and P. G. Simpkins, "Laser Speckle Photography in a Fluid Medium," Nature London **270,** 45 (1977).
4. R. Meynart, "Instantaneous Velocity Field Measurements in Unsteady Gas Flow by Speckle Velocimetry," Appl. Opt. **22,** 535 (1983).
5. R. J. Adrian, "Scattering Particle Characteristics and Their Effect on Pulsed Laser Measurements of Fluid Flow: Speckle Velocimetry vs Particle Image Velocimetry," Appl. Opt. **23,** 1690 (1984).
6. C. J. D. Pickering and N. A. Halliwell, "Laser Speckle Photography and Particle Image Velocimetry: Photographic Film Noise," Appl. Opt. **23,** 2961 (1984).
7. W. Lauterborn and A. Vogel, "Modern Optical Techniques in Fluid Mechanics," Annu. Rev. Fluid Mech. **16,** 223 (1984).
8. F. Durst, A. Melling, and J. H. Whitelaw, *Principles and Practice of Laser-Doppler Anemometry* (Academic, London, 1976).
9. L. E. Drain, *The Laser Doppler Technique* (Wiley, New York, 1980).
10. T. B. Benjamin and A. T. Ellis, "The Collapse of Cavitation Bubbles and the Pressures Thereby Produced Against Solid Boundaries," Philos. Trans. R. Soc. London Ser. A **260,** 221 (1966).
11. W. Lauterborn, "Kavitation durch Laserlicht," Acustica **31,** 51 (1974).
12. J. R. Blake and D. C. Gibson, "Cavitation Bubbles Near Boundaries," Annu. Rev. Fluid Mech. **19,** 99 (1987).
13. Y. Tomita and A. Shima, "Mechanisms of Impulsive Pressure Generation and Damage Pit Formation by Bubble Collapse," J. Fluid Mech. **169,** 535 (1986).
14. W. Lauterborn and W. Hentschel, "Cavitation Bubble Dynamics Studied by High Speed Photography and Holography: Part One," Ultrasonics **23,** 260 (1985).
15. M. S. Plesset and R. B. Chapman, "Collapse of an Initially Spherical Vapour Cavity in the Neighborhood of a Solid Boundary," J. Fluid Mech. **47,** 283 (1971).
16. J. R. Blake, B. B. Taib, and G. Doherty, "Transient Cavities Near Boundaries. Part 1. Rigid Boundary," J. Fluid Mech. **170,** 479 (1986).
17. R. J. Adrian, "Image Shifting Technique to Resolve Directional Ambiguity in Double-Pulsed Velocimetry," Appl. Opt. **25,** 3855 (1986).
18. L. Lourenco, "Theory and Applications of Particle Image Displacement Velocimetry," in *Lecture Series 1986-09*, von Karman Institute for Fluid Dynamics (Brussels, 1986), p. 1.
19. C. S. Moraitis, M. L. Riethmüller, J. M. Buchlin, and N. Selfslagh, "Computer Processing of Fringe Patterns for Laser Speckle Velocimetry," in *Lecture Series 1986-09*, von Karman Institute for Fluid Dynamics (Brussels, 1986), p. 53.
20. K. A. Marko and L. Rimai, "Video Recording and Quantitative Analysis of Seed Particle Track Images in Unsteady Flows," Appl. Opt. **24,** 3666 (1985).
21. R. E. Elkins, G. R. Jackman, R. R. Johnson, E. R. Lindgren, and J. K. Yoo, "Evaluation of Stereoscopic Trace Particle Records of Turbulent Flow Fields," Rev. Sci. Instrum. **48,** 738 (1977).
22. T. Kobayashi, T. Saga, and S. Segawa, "Some Considerations on Automated Image Processing of Pathline Photographs," in *Pro-*

ceedings, *Fourth International Symposium on Flow Visualization*, Paris (1986), paper B3.1.
23. P. E. Dimotakis, F. D. Debussy, and M. M. Koochesfahani, "Particle Streak Velocity Field Measurements in a Two Dimensional Mixing Layer," Phys. Fluids **24**, 955 (1981).
24. K. Imaichi and K. Ohmi, "Quantitative Flow Analysis by Image Processing of Flow Visualization Photographs," in *Flow Visualization III*, W. J. Yang, Ed. (Hemisphere, Washington, 1985), p. 301.
25. T. Kobayashi, T. Ishihara, and T. Sasaki, "Automatic Analysis of Photographs of Trace Particles by Microcomputer System," in *Flow Visualization III*, W. J. Yang, Ed. (Hemisphere, Washington, 1985), p. 231.
26. W. Lauterborn and H. Bolle, "Experimental Investigations of Cavitation Bubble Collapse in the Neighborhood of a Solid boundary," J. Fluid Mech. **72**, 391 (1975).
27. Chemische Werke Hülls, D-4370 Marl, Federal Republic of Germany, Data Sheet "Vestamid X 3694" (Hüls, 1983).
28. R. J. Adrian and C. S. Yao, "Pulsed Laser Technique Application to Liquid and Gaseous Flows and the Scattering Power of Seed Materials," Appl. Opt. **24**, 44 (1985).
29. J. R. Blake, U. Wollongong, Australia; personal communication.

Meetings *continued from page 1707*

1988
October

16–21 11th Triennial World Cong. of the Int. Measurement Confederation & the 43rd Ann. Conf. & Exhibition of the Instrument Soc. Am., Houston *IMEKO Secretariat, P.O.B. 457, H-1371 Budapest, Hungary*

17–21 Laser Safety: Hazards, Inspection & Control course, San Francisco *Laser Inst. Amer., 5151 Monroe St., Toledo, OH 43623*

30–4 Nov. Factors Influencing the Efficiency of Photographic Imaging East–West Symp. 2, Kona *SPSE, 7003 Kilworth Lane, Springfield, VA 22151*

30–4 Nov. **OPTCON'88,** Santa Clara *OSA Mtgs. Dept., 1816 Jefferson Pl., NW, Wash., DC 20036*

31–2 Nov. 8th Int. Photopolymer Conf.: Principles, Processes & Materials, Ellenville, NY *P. Shah, C/O IBM Corp., D/959-40E, Rt. 52, Hopewell Junction, NY 12533*

31–4 Nov. **Applications of Optical Engineering Mtg.,** Santa Clara *OSA Mtgs. Dept., 1816 Jefferson Pl., NW, Wash., DC 20036*

31–4 Nov. APS Division of Plasma Phys. Mtg., Hollywood *APS, 335 E. 45th St., New York, NY 10017*

31–4 Nov. **OSA Ann. Mtg., Santa Clara** *OSA Mtgs. Dept., 1816 Jefferson Pl., NW, Wash., DC 20036*

31–2 Nov. 7th Int. Congr. on Applications of Lasers & Electro-Optics, Santa Clara *Laser Inst. of Amer., 5151 Monroe St., Toledo, OH 43623*

November

1–4 **OSA Workshop on Optical Fabrication & Testing,** Santa Clara *OSA Mtgs. Dept., 1816 Jefferson Pl., NW, Wash., DC 20036*

2–4 LEOS Ann. Mtg., Santa Clara *LEOS/IEEE, 345 E. 47th St., New York, NY 10017*

2–4 3rd Int. Conf. on Polyimides, Ellenville, NY *P. Shah, C/O IBM Corp., D/959-40E, Rt. 52, Hopewell Junction, NY 12533*

4–7 5th Int. Retinitis Pigmentosa Congr., Melbourne *Conf. Sec., 46A Oxley Rd., Hawthorn 3122, Victoria, Australia*

6–11 Cambridge Symp. on Advances in Intelligent Robotics Systems, Cambridge *SPIE, P.O. Box 10, Bellingham, WA 98227*

7–10 Int. Cong. on Applications of Lasers & Electro-Optics, Orlando *Laser Inst. Am., 5151 Monroe St., Toledo, OH 43623*

7–11 Visual Communications & Image Processing III, Cambridge *SPIE, P.O. Box 10, Bellingham, WA 98827*

9–11 Optical Storage for Small Systems Mtg., Los Angeles *TOC, P.O. Box 14817, San Francisco, CA 94114*

13–17 Biostereometrics Mtg., Basel *SPIE, P.O. Box 10, Bellingham, WA 98827*

28–3 Dec. Materials Research Soc. Mtg., Boston *MRS, 9800 McKnight Rd., Ste. 327, Pittsburgh, PA 15237*

December

5–9 Int. Conf. on Lasers, Lake Tahoe *Soc. for Optical & Quantum Electronics, Lasers'88, P.O. Box 245, McLean, VA 22101*

12–17 Int. Workshop on Advances in Holography & Speckle Phenomenon & Their Industrial Applications, Madras *R. Sirohi, HOSPIA, Eng. Design Ctr., Indian Inst. Tech., Madras-600 036, India*

19–21 6th Mtg. Optical Eng. in Israel, Tel Aviv *SPIE, P.O. Box 10, Bellingham, WA 98227*

1989
January

15–20 O-E/LASE '89 Optoelectronics & Laser Applications in Sci. & Eng. course, Los Angeles *SPIE, P.O. Box 10, Bellingham, WA 98227*

17–20 **Optical Data Storage Top. Mtg.,** Los Angeles *OSA Mtgs. Dept., 1816 Jefferson Pl., NW, Wash., DC 20036*

29–3 Feb. Medical Imaging III, Newport Beach *SPIE, P.O. Box 10, Bellingham, WA 98227*

continued on page 1893